Available online at www.sciencedirect.com
SCIENCE DIRECT®
ELSEVIER
International Journal of Mechanical Sciences 47 (2005) 902–921
International Journal of MECHANICAL SCIENCES
www.elsevier.com/locate/ijmecsci

An analysis of force distribution in shear spinning of cone

Ming-Der Chen[a], Ray-Quan Hsu[a,*], Kuang-Hua Fuh[b]

[a]*Department of Mechanical Engineering, National Chiao Tung University, 1001 Ta-Hsueh Road, 300 Hsinchu, Taiwan*
[b]*Department of Mechanical and Marine Engineering, National Taiwan Ocean University, Taiwan*

Received 1 July 2003; received in revised form 20 December 2004; accepted 21 January 2005
Available online 7 April 2005

Abstract

An analytic model for calculation of shear spinning force incorporate factor of over-roll (press down) of the blank is derived. The effects of blank thickness, roller nose radius, mandrel revolution and roller feed on the spinning force are discussed. Results obtained from calculation were compared with the experiment and other theoretical predictions. It is found that the present findings yield optimum results.

Keywords: Shear spinning; Shear force; Spun cone; Surface roughness; Over-roll depth

1. Introduction

Shear spinning is a technique for manufacturing cone shape products by virtue of a roller and a rotating male form. As shown in Fig. 1, conical parts are produced by pressing the spinning roller on to the sheet blank which in turn is mounted on a rotating mandrel. Under the pressure of the roller, the material is axially displaced whereby the blank thickness is reduced. In this process, radial-axis position of the blank element was considered fix during deformation as depicted in Fig. 1.

Shear spinning process is adopted by the industry for manufacturing dished ends for boilers and tanks, wheel rims, silencer parts, nozzle, etc. As indicated by Held [1], in the spinning process, the roller press a small depth on the blank, over-roll, is important to confirm the accuracy of shape

*Corresponding author. Tel.: +886 35 712121; fax: +886 35 720634.
E-mail address: rqhsu@mail.nctu.edu.tw (R.-Q. Hsu).

0020-7403/$ - see front matter
doi:10.1016/j.ijmecsci.2005.01.010

Nomenclature

Cs	over-roll depth (mm)
f	roller feed (mm/rev)
w	specific deformation energy (N-mm/mm^3)
$\mathrm{d}v$	strained metal volume (mm^3)
$\Delta\overline{\varepsilon_{ii}}$; $\mathrm{d}\bar{\varepsilon}$	increment of normal strain due to bending, infinitesimal effective strain
$\overline{\sigma_m}$; $\bar{\sigma}$	mean effective stress; effective stress (N/mm^2)
R, θ, Z	cylindrical co-ordinates
X, Y, Z	rectangular co-ordinates
γ	fraction
ρ_R	roller nose radius (mm)
ρ_n	radius of curvature (mm)
h	distance of a point from the neutral surface in the thickness direction (mm)
t_0; t_f	original; final thickness of blank (mm)
N	mandrel revolution, (rev/min)
α	half-apex angle of mandrel (deg)
ψ	roller contact angle (deg)
θ_0; $\overline{\theta_0}$	deformation zone angle and its average value (rad)
θ_0'; $\overline{\theta_0'}$	angle functionally related to θ_0 and $\overline{\theta_0}$ (rad)
υ_1; υ_2	ratios of strains
D_R	roller diameter (mm)
A_t; A_r; A_z	deformation areas of the contact surface between roller and cone in circumferential, radial, and axial directions, respectively (mm^2)
F_p; F_q	force components in parallel and perpendicular directions to the roller axis, respectively (N)
F_r; F_z	force components in the radial and axial directions, respectively (N)
F_t	circumferential force components (N)

and dimensions, on the other hand, the over-roll can eliminate the rough surface of the blank material and produce the new surface on finished part. A way to estimate forces required for the process incorporating the over-roll of blank thus is essential for the design of the tool and selection of the machinery.

Hayama et al. [2] did consider five factors namely diameter of mandrel, corner radius of mandrel, roller diameter, roller nose radius and mandrel rotation to determine the pass schedule of roller. They also investigated experimental results of three force components with respect to stroke, blank thickness, conic angle and roller feed [3], however, no equation for spinning force calculation related to spinning parameters were proposed.

Avitzur and Yang [4] first derived the tangential force equation for spinning of cones. They also showed an approximate method to calculate the power. Kalpakcioglu [5] developed the tangential force and the specific energy equations under the assumption of simple shear deformation. Kobayashi and Thomsen [6] derived the tangential force equation assuming that the infinitesimal

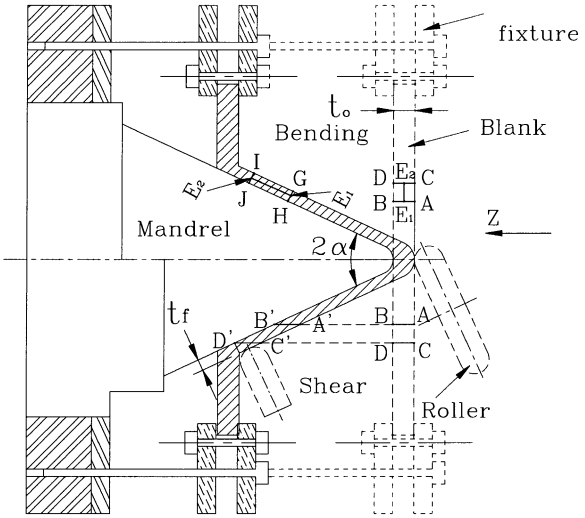

Fig. 1. Bending and shear deformation of a blank in spinning.

strain ratios remain constant during the spinning process. The radial and axial force components were calculated by using the projected contact area ratios.

However, all the studies stated above concerned only the power consumption in spinning of cones, the effect of individual spinning parameters on the spinning forces were never discussed. In this study, the effects of blank thickness, roller nose radius, mandrel revolution, roller feed and over-roll depth on the spinning forces are taken into consideration and incorporated in the proposed equations. Predictions calculated from the equations are compared with the experimental results. It is observed that the proposed equations yield the better results.

2. Analysis of shear spinning process

As depicted in Fig. 1, in the process of shear spinning, the spinning roller presses on a rotating sheet blank, force it to conform with the contour of the mandrel. Deformation of the sheet blank in this process is a combination of bending and shearing. In the course of forming, it is assumed that the radial distance of any point on the neutral line (point E_1 or E_2) remains unchanged, and the line sections AB and CD in Fig. 1 hold straight and normal to the surface throughout the deformation. It means that after bending, the neutral line section E_1E_2 is also perpendicular to line sections GH and IJ. On the other hand, any point within the blank is assumed to retain its radial distance in shearing. Line sections AB and CD change to $A'B'$ and $C'D'$ and still hold parallel to the Z-axis. Besides, $AB = A'B'$ and $CD = C'D'$ [4,6].

In addition, the following assumptions were adopted:

1. The material is homogeneous, isotropic rigid-plastic body, without Bauschinger effect and volumetric change and non-strain hardening.
2. Material follows von Mises yield rule.

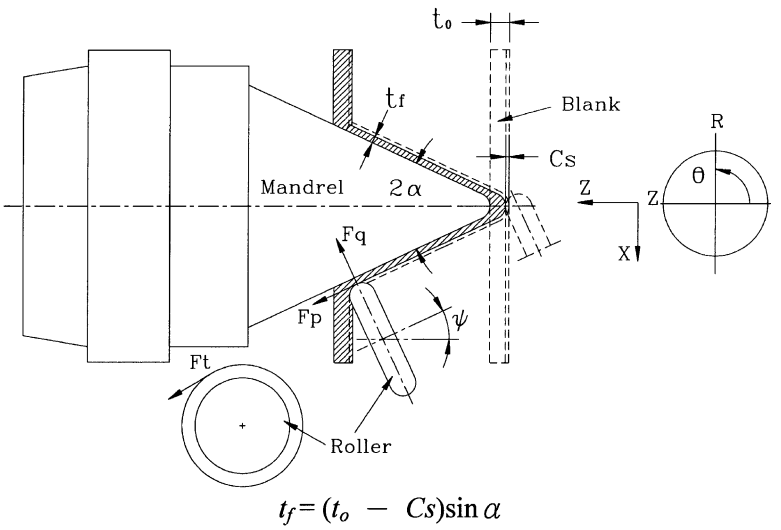

Fig. 2. Thinning of the blank in shear spinning.

3. The frictional force between roller and blank is negligible, strain rate effects and temperature effects are also neglected.

As shown in Fig. 2, the initial blank thickness t_0 and final thickness t_f can be related by the following correlation, known as the sine law in shear spinning:

$$t_f = (t_0 - Cs)\ \sin\ \alpha, \tag{1}$$

here Cs is over-roll depth and α is half-cone angle. The force applied by the roller on the blank can be resolved into three mutually perpendicular components, the circumferential force, F_t, feed force, F_p, and the radial force, F_q (perpendicular to F_p). The order of their magnitude as pointed out by Avitzur and Kegg is $F_q > F_p > F_t$ [4,7]. The largest of the three F_q, however, does no work at all, because it is not associated with any displacement. The displacement in the direction of F_p is small compared with the circumferential direction ($f\ \sin\ \alpha\,(\mathrm{mm/rev.}) \ll 2\pi R\,(\mathrm{mm/rev.})$), thus the work done by the force F_p can be neglected compared with the work done by F_t. Hence, most of the power supplied by the motor driving the chuck of the spinning machine is transmitted into torque through the circumferential force F_t [4]. Thus, the external work input is approximated by $F_t\,\mathrm{d}l$, where $\mathrm{d}l$ is the roller displacement during an infinitesimal time interval $\mathrm{d}t$. On the other hand, the total deformation work in an infinitesimal time interval is expressed by

$$\mathrm{d}W = w\,\mathrm{d}v, \tag{2}$$

where w is the specific work (work of deformation per unit volume) and $\mathrm{d}v$ is the volume of the blank which was strained in the same time interval. Equating the external work input to the work of deformation given by Eq. (2), permits the following energy balance:

$$F_t\,\mathrm{d}l \cong w\,\mathrm{d}v = \mathrm{d}v \int \bar{\sigma}\,\mathrm{d}\bar{\varepsilon}, \tag{3}$$

where $\bar{\sigma}$ and $\mathrm{d}\bar{\varepsilon}$ are effective stress and infinitesimal effective strain, respectively. Eq. (3) can also be written as

$$F_t = \frac{\mathrm{d}v}{\mathrm{d}l}\int \bar{\sigma}\,\mathrm{d}\bar{\varepsilon} = (t_0 - Cs)\,\sin\alpha f \int \bar{\sigma}\,\mathrm{d}\bar{\varepsilon} = A_t \int \bar{\sigma}\,\mathrm{d}\bar{\varepsilon}, \tag{4}$$

where f is the roller feed. A_t is the circumferential contact area of roller and blank.

2.1. Finite strain

The strain rates of deformation in cylindrical polar coordinates (R, θ, Z) assume the form (see Fig. 2):

$$\dot{\varepsilon}_{RR} = \frac{\partial \dot{u}_R}{\partial R}, \quad \dot{\varepsilon}_{\theta\theta} = \frac{1}{R}\frac{\partial \dot{u}_\theta}{\partial \theta} + \frac{\dot{u}_R}{R}, \quad \dot{\varepsilon}_{ZZ} = \frac{\partial \dot{u}_Z}{\partial Z},$$

$$\dot{\varepsilon}_{R\theta} = \frac{\partial \dot{u}_\theta}{\partial R} + \frac{1}{R}\frac{\partial \dot{u}_R}{\partial \theta} - \frac{\dot{u}_\theta}{R},$$

$$\dot{\varepsilon}_{\theta Z} = \frac{1}{R}\frac{\partial \dot{u}_Z}{\partial \theta} + \frac{\partial \dot{u}_\theta}{\partial Z},$$

$$\dot{\varepsilon}_{RZ} = \frac{\partial \dot{u}_Z}{\partial R} + \frac{\partial \dot{u}_R}{\partial Z}, \tag{5}$$

where $\dot{\varepsilon}_{RR}, \dot{\varepsilon}_{\theta\theta}, \dot{\varepsilon}_{ZZ}, \dot{\varepsilon}_{R\theta}, \dot{\varepsilon}_{\theta Z}$ and $\dot{\varepsilon}_{RZ}$ are the components of the normal strain-rate tensor field, $\dot{u}_R$, $\dot{u}_\theta$ and $\dot{u}_Z$ are the components of velocity-vector field.

Total effective plastic strain increment $\mathrm{d}\overline{\varepsilon_p}$, which is proportional to the root mean square of the differences of the principal plastic strain increments and shear strain takes the form of

$$\mathrm{d}\overline{\varepsilon_p} = \left\{\tfrac{2}{9}[(\mathrm{d}\varepsilon_{RR} - \mathrm{d}\varepsilon_{\theta\theta})^2 + (\mathrm{d}\varepsilon_{\theta\theta} - \mathrm{d}\varepsilon_{ZZ})^2 + (\mathrm{d}\varepsilon_{\theta\theta} - \mathrm{d}\varepsilon_{RR})^2] + \tfrac{1}{3}[\mathrm{d}\varepsilon_{R\theta}^2 + \mathrm{d}\varepsilon_{\theta Z}^2 + \mathrm{d}\varepsilon_{RZ}^2]\right\}^{1/2}. \tag{6}$$

Because the angular velocity of the spun cone is constant, the circumferential velocity at any point on the cone becomes

$$\dot{u}_\theta = 2\pi RN, \tag{7}$$

where $\dot{u}_\theta$ is the circumferential velocity (mm/min), R the radius at the point considered (mm) and N the rotation of the blank per minute (rev/min).

Also, since there is no radial displacement for any point on the cone during spinning, the radial velocity $\dot{u}_R$ will be:

$$\dot{u}_R = 0. \tag{8}$$

The geometry of contact area between roller and blank in Z-axis can be expressed in the following form:

$$Z = F(R, \theta, n). \tag{9}$$

Then

$$dZ = \frac{\partial Z}{\partial R}\,dR + \frac{\partial Z}{\partial \theta}\,d\theta + \frac{\partial Z}{\partial n}\,dn \tag{10}$$

and

$$\dot{u}_Z = \frac{dZ}{dT} = \frac{\partial Z}{\partial R}\frac{dR}{dT} + \frac{\partial Z}{\partial \theta}\frac{d\theta}{dT} + \frac{\partial Z}{\partial n}\frac{dn}{dT}, \tag{11}$$

where n is the number of revolutions passed from time T_0 to the instant, T the time passed from T_0 to the instant and $\dot{u}_Z$ the velocity component in Z-direction.

Now

$$n = N(T - T_0), \quad \frac{dn}{dT} = N, \tag{12}$$

$$\frac{d\theta}{dT} = \frac{\dot{u}_\theta}{R} = 2\pi N, \tag{13}$$

$$\frac{dR}{dT} = \dot{u}_R = 0. \tag{14}$$

Thus, Eq. (11) can be simplified

$$\begin{aligned}\dot{u}_Z &= \frac{\partial Z}{\partial \theta}2\pi N + \frac{\partial Z}{\partial n}N \\ &= N\left(2\pi\frac{\partial Z}{\partial \theta} + \frac{\partial Z}{\partial n}\right).\end{aligned} \tag{15}$$

Replace (7), (8), (13) and (14), into (5), it becomes

$$\dot{\varepsilon}_{RR} = 0, \quad \dot{\varepsilon}_{\theta\theta} = \frac{1}{R}\frac{\partial \dot{u}_\theta}{\partial \theta}, \quad \dot{\varepsilon}_{ZZ} = \frac{\partial \dot{u}_Z}{\partial Z},$$

$$\dot{\varepsilon}_{R\theta} = 0,$$

$$\dot{\varepsilon}_{\theta Z} = \frac{1}{R}\frac{\partial \dot{u}_Z}{\partial \theta},$$

$$\dot{\varepsilon}_{RZ} = \frac{\partial \dot{u}_Z}{\partial R}. \tag{16}$$

Fig. 3 is a radial view of roller/blank interaction. Where ρ is the radius of curvature of blank/roller contact line PQ and h is the distance of a point in the thickness-direction from the neutral surface (see the right side of Fig. 3). Suppose $h \ll \rho_n$ and $\rho \cong \rho_n + h$, where ρ_n is the radius of the curvature P_nQ_n, then the bending strain $\Delta\varepsilon_\alpha \cong h/\rho$ [8], since it may be assumed that $\Delta\varepsilon_\alpha \cong \Delta\varepsilon_{\theta\theta}$, by the fact of $\Delta\varepsilon_{RR} = 0$, therefore, $\Delta\varepsilon_{\theta\theta}$ is equivalent to h/ρ. The state of strain at point due

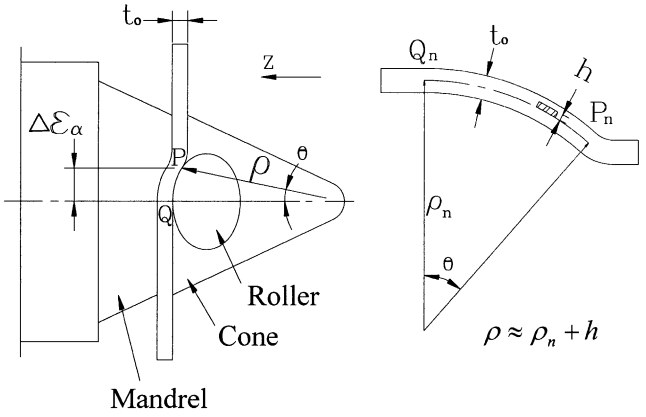

Fig. 3. Radial view of roller/blank contact.

to bending is given by

$$\Delta\varepsilon_{\theta\theta} = -\Delta\varepsilon_{ZZ} \cong \frac{h}{\rho} \cong \frac{t_0}{4\rho_n}.$$

Substitution of Eq. (16) into Eq. (6) yields:

$$\mathrm{d}\overline{\varepsilon_p} = \left\{\tfrac{2}{9}(6\Delta\varepsilon_{\theta\theta}^2) + \tfrac{1}{3}(\Delta\varepsilon_{\theta Z}^2 + \Delta\varepsilon_{RZ}^2)\right\}^{1/2},$$

$$\mathrm{d}\varepsilon_p = \frac{1}{\sqrt{3}}\Delta\varepsilon_{RZ}[(1+\upsilon_1^2+\upsilon_2^2)^{1/2}],$$

where

$$\upsilon_1 = \frac{\Delta\varepsilon_{\theta\theta}}{\Delta\varepsilon_{RZ}/2},$$

$$\upsilon_2 = \frac{\Delta\varepsilon_{\theta Z}}{\Delta\varepsilon_{RZ}}. \tag{17}$$

Moreover, the strain $\Delta\varepsilon_{\theta Z}$ of Eq. (16) in Fig. 4 can be rewritten as

$$\Delta\varepsilon_{\theta Z} = \frac{1}{R}\Delta\left(\frac{\partial u_z}{\partial\theta}\right) = \tan\delta, \quad \tan\delta \Rightarrow \tan\delta' \tag{18}$$

where δ' is the angle between the tangent to the blank/roller contact curve $P_n'Q_n'Q_n''$ and the horizontal line at point Q_n' on Fig. 4. Assuming the curve P_nQ_n is an arc with radius ρ_n, its center is located on the Z'-axis, and by neglecting the term $(\gamma Z_n')^2$ as compared with $(R_n\theta_0')^2$ (Appendix A). We obtain

$$\rho_n \cong \frac{(R_n\theta_0)^2}{2Z_n'}, \tag{19}$$

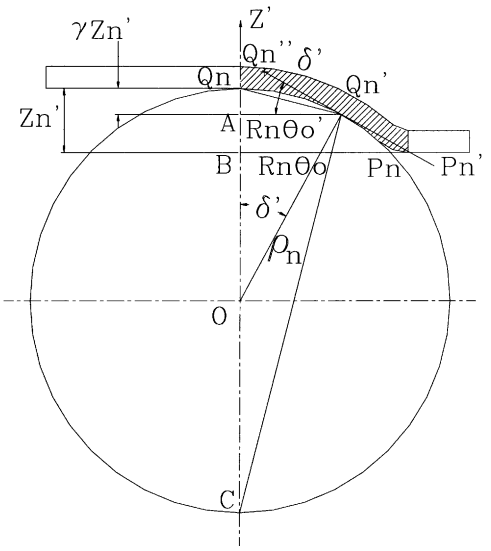

Fig. 4. Straining of an element.

$$\tan \delta' \cong \frac{2Z'_n}{R_n\theta_0}. \tag{20}$$

Noting that

$$\sum_1^{n_0} Z'_n = \rho_R\left(\frac{1}{\sin\,\alpha} - 1\right), \tag{21}$$

$$\sum_1^{n_0} \Delta\varepsilon_{RZ} = \cot\,\alpha \tag{22}$$

and combining Eqs. (18)–(22),

$$\Delta\varepsilon_{\theta\theta} = \frac{t_0/2}{(R_n\overline{\theta}_n)^2}\rho_R\left(\frac{1-\sin\,\alpha}{\sin\,\alpha}\right), \tag{23}$$

$$\Delta\varepsilon_{\theta Z} = \frac{2}{R_n\overline{\theta}_0}\rho_R\left(\frac{1-\sin\,\alpha}{\sin\,\alpha}\right). \tag{24}$$

Here, $\overline{\theta_0}$ is the angle of the roller/blank contact line as projected on to the $R-\theta$ plane given by Fig. 5:

$$\overline{\theta_0} = \cos^{-1}\left[\frac{\frac{b^2}{a^2} - \sqrt{1+(\frac{b}{R_0})^2(\frac{b^2}{a^2}-1)}}{\frac{b^2}{a^2}-1}\right], \tag{25}$$

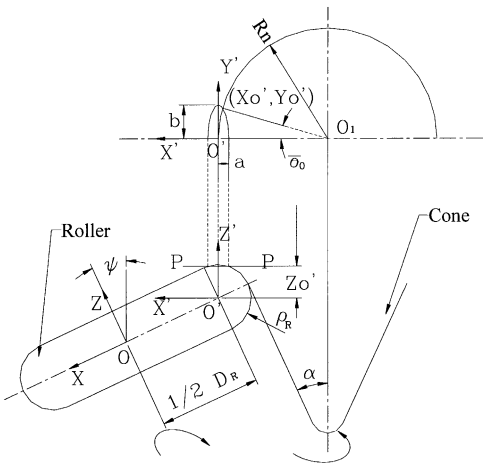

Fig. 5. Roller/blank contact area.

where

$$a = \sqrt{\rho_R^2 - (\rho_R - f\,\cos\,\alpha)^2},$$

$$b^2 = D_R\left\{\sqrt{\rho_R^2 - [(\rho_R - f\,\cos\,\alpha)\cos\,\psi]^2} - [(\rho_R - f\,\cos\,\alpha)\sin\,\psi]\right\} + \rho_R^2 - (\rho_R - f\,\cos\,\alpha)^2 \tag{26}$$

and ρ_R is the roller nose radius, D_R is the roller diameter, α is one half the cone angle, $R_n = (R_i + R_0)/2 = R_0 - (\rho_R \cos\,\alpha/2)$, and ψ is the roller contact angle, respectively (Appendix B).

Combining Eqs. (22)–(24), substituting into Eq. (17), the total effective strain $\int \mathrm{d}\bar{\varepsilon}$ becomes

$$\int \mathrm{d}\overline{\varepsilon_p} = \sum_1^{n_0} \Delta\overline{\varepsilon_n} = \frac{\cot\,\alpha}{\sqrt{3}}(1 + \upsilon_1^2 + \upsilon_2^2)^{1/2}, \tag{27}$$

$$\upsilon_1 = \frac{t_0}{(R_n\overline{\theta_0})^2}\rho_R\left(\frac{1 - \sin\,\alpha}{\cos\,\alpha}\right),$$

where

$$\upsilon_2 = \frac{2}{R_n\overline{\theta_0}}\rho_R\left(\frac{1 - \sin\,\alpha}{\cos\,\alpha}\right).$$

2.2. Spinning force

In the experiment, the circumferential, parallel and perpendicular force components F_t, F_p and F_q, respectively, were measured by three-channel dynamometer. The shear spinning force on the

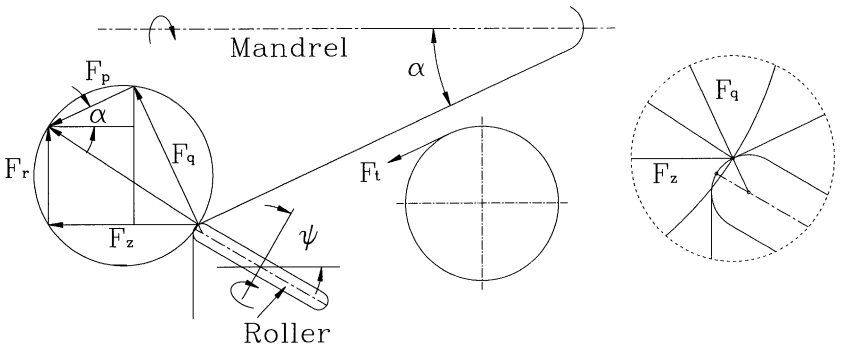

Fig. 6. Spinning force components.

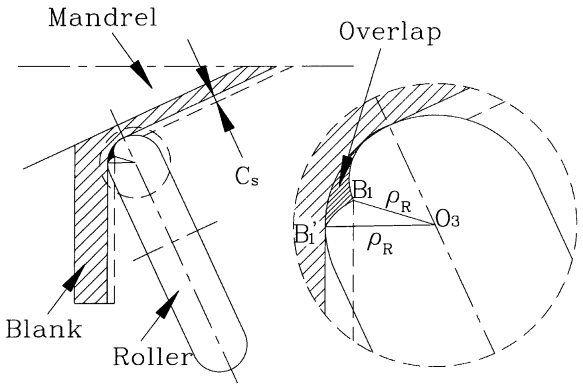

Fig. 7. Overlap of the blank material on the roller.

roller can be resolved into three mutually perpendicular components as the F_t (circumferential), F_r (radial) and F_z (axial) as indicated by Fig. 6.

Force components F_r and F_z are related to F_p and F_q by

$$F_r = F_q \cos\alpha - F_p \sin\alpha, \tag{28}$$

$$F_z = F_q \sin\alpha + F_p \cos\alpha. \tag{29}$$

Therefore, the force components F_r and F_z can be calculated from measured force components F_p and F_q and half-cone angle. Circumferential force F_t is measured by dynamometer directly.

In shear spinning process, the over-roll on blank thickness is adjusted to obtain the required surface roughness. In practice, when the roller set an amount of over-roll on the blank, it will cause a small portion of blank material curl-up to envelope the outer rim of roller nose as indicated in Fig. 7. To simplify the analysis, the power consumed by this curl-up deformation is neglected.

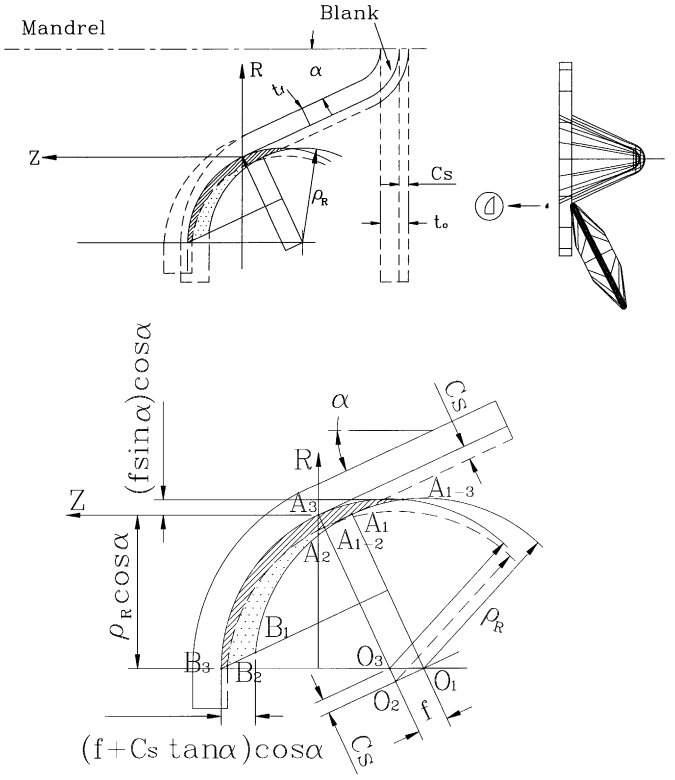

Fig. 8. Details of roller/blank contact area on circumferential view.

2.3. Contact deformation area

Fig. 8 depicts the circumferential deformation area of roller and blank in shear spinning process. Details of the deformation area with reduction in blank thickness (over-roll) is shown in the lower part of the drawing. When a roller is moving with a constant feed f and an over-roll depth Cs, the roller/blank contact point is changing from A_1 to A_2, and A_3 finally. The radial component of $\overline{A_{1-3}A_3}$ is equal to $(f \sin\alpha)\cos\alpha$. When no over-roll of the blank is performed in the process, points B_1, B_2 are the first contact points of the roller with the blank flange at one feed apart, respectively. Hence, in the case where no over-roll is taken place, the deformation area is the domain enclosed by the dots section $(A_{1-2}B_1)$, $(A_{1-2}B_2)$ and (B_1B_2). When over-roll of the blank is performed, point B_3 becomes the final contact point after a feed. The amount of deformation area increased in the case where over-roll exists is indicated by the cross hatching. The distance $\overline{B_1B_3}$ in the axial direction is computed as

$$(\overline{B_1B_3})_Z \cong (f + Cs\tan\alpha)\cos\alpha. \tag{30}$$

Therefore, the total contact areas indicated by dotted hatch in Fig. 8 can be approximately computed as follows:

$$A_t \cong \tfrac{1}{2}(f + Cs \tan \alpha) \cos \alpha(\rho_R \cos \alpha + f \sin \alpha \cos \alpha). \tag{31}$$

On the other hand, Fig. 9 presents the radial contact area of roller and blank. On the left side of the drawing is a magnified details of the contact area. The area can be calculated approximately as follows:

$$A_r \cong \tfrac{1}{2}(f + Cs \tan \alpha) \cos \alpha \tfrac{1}{2} D_R \overline{\theta_0}, \tag{32}$$

where D_R is the roller diameter (mm).

Similarly, Fig. 10 illustrates the axial contact area of roller and blank flange. Magnification of this area is presented on left side of the drawing. Same as above, the area is approximately

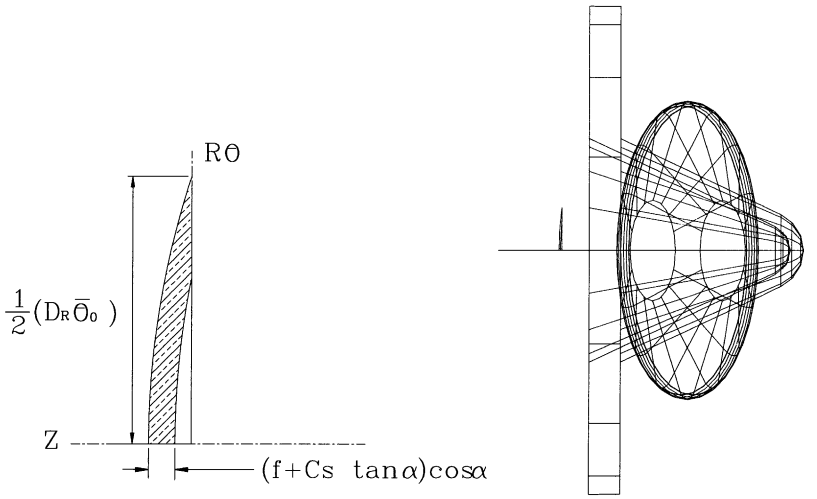

Fig. 9. Radial view of the roller/blank contact area.

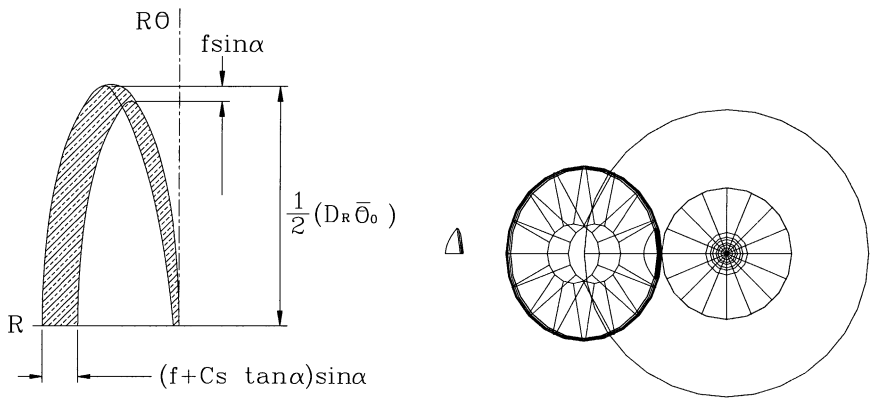

Fig. 10. Axial view of the roller/blank contact area.

calculated as follows:

$$A_z \cong \tfrac{3}{2}(f + Cs \tan \alpha) \sin \alpha \tfrac{1}{2} D_R \overline{\theta_0} \tag{33}$$

Substitute Eq. (31) into Eq. (4), we obtain the circumferential force as follows:

$$F_t \cong \tfrac{1}{2}(f + Cs \tan \alpha) \cos \alpha (\rho_R \cos \alpha + f \sin \alpha \cos \alpha) \left(\overline{\sigma_m} \int \mathrm{d}\bar{\varepsilon} \right), \tag{34}$$

where $\overline{\sigma_m}$ and $\bar{\varepsilon}$ are the mean effective stress and strain.

Furthermore, the radial and axial force F_r and F_z can be expressed as following:

$$F_r \cong \tfrac{1}{4}(f + Cs \tan \alpha) \cos \alpha (D_R \overline{\theta_0}) \left(\overline{\sigma_m} \int \mathrm{d}\bar{\varepsilon} \right), \tag{35}$$

$$F_z \cong \tfrac{3}{4}(f + Cs \tan \alpha) \sin \alpha (D_R \overline{\theta_0}) \left(\overline{\sigma_m} \int \mathrm{d}\bar{\varepsilon} \right). \tag{36}$$

3. Experimental set-up

Fig. 11 presents the schematic diagram of shear spinning experimental set-up and spinning force measuring system. A modified CNC spinning device is driven by a 15 hp DC motor on its spindle, and longitudinal and latitude power rates are 5 and 3 hp, respectively. A special fixture holds the blank at its rim and, can move concurrently with roller. A three-channel dynamometer (Kistler 9257A) measures the shear spinning force. The force output signals were amplified through a

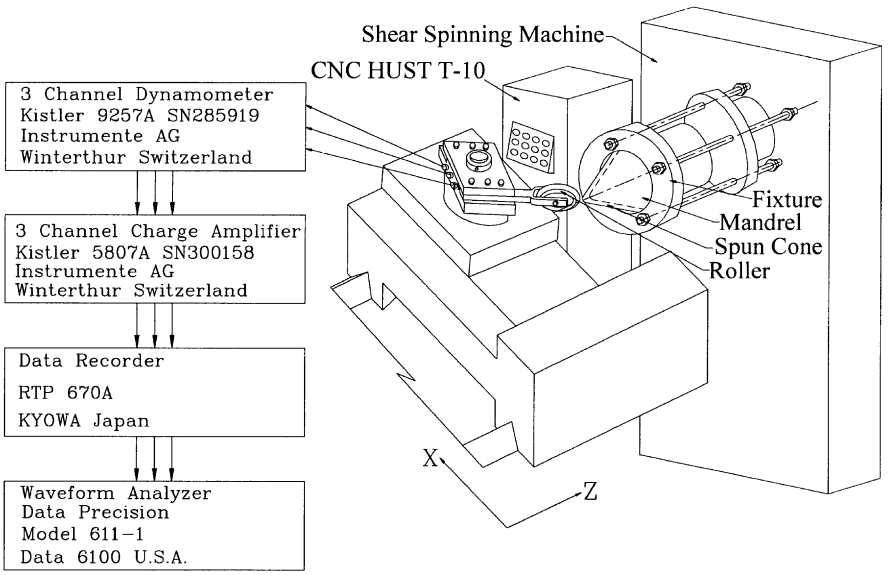

Fig. 11. A schematic diagram of shear spinning equipment and spinning force measuring system.

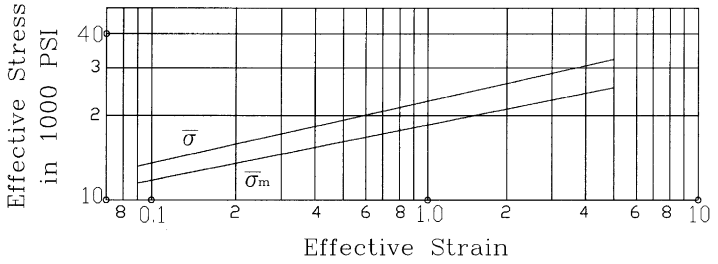

Fig. 12. Mean effective strain–stress curve for aluminum 1100-O [6].

Table 1
The experimental conditions employed in spinning

Blank thickness, t_0 (mm)	1.5; 2.59; 4.11; 6.0; 7.0	A1-1100-O
Roller nose radius, ρ_R (mm)	2.5; 4.0; 4.8; 5.5; 7.1	SAE 4130
Mandrel revolution, N (rev/min)	40; 60	
Roller feed, f (mm/rev)	0.1; 0.13; 0.16; 0.18; 0.2	
Over-roll depth, Cs (mm)	0.3; 0.4; 0.5; 0.6; 0.7	
Cone angle, α (deg)	50	
Roller contact angle, ψ (deg)	60	

three-channel charge amplifier (Kistler 5807A). For the convenience of analysis, a data recorder (KYOWA RTP 670A) was connected to the charge amplifier. The recorded data were carefully analyzed through a waveform analyzer (Data Precision Model 6100). A CNC control unit adjusts the mandrel revolution and roller feed. The shear spinning processes can be executed through a numerical control program. Material selected for the experiment is Al 1100-O and its mean effective stress $\overline{\sigma_m}$ and strain $\bar{\varepsilon}$ relationship is illustrated on Fig. 12. The experimental conditions employed in spinning are given in Table 1.

4. Results and discussion

Fig. 13 depicts the three force components as measured in the experiments. The experiments were repeated ten times. The axial force F_z is the largest among three components ($F_z > F_r > F_t$). Fig. 14 expresses the force components F_t, F_r and F_z as function of blank thickness. For $\rho_R = 4.8\,\text{mm}$, $N = 60\,\text{rev/min}$, $f = 0.16\,\text{mm/rev}$ and $Cs = 0.5\,\text{mm}$, the experimental values are indicated by solid dots, calculated results from Eqs. (34)–(36) are shown by solid lines. The results by Kobayashi and Thomsen [6] and Kegg [7], which only F_t is proposed are also shown for the purpose of comparison. Obviously, the predictions derived from Eqs. (34)–(36), which take into consideration the factor of over-roll (Cs) is in better accordance with the experiments. The reason

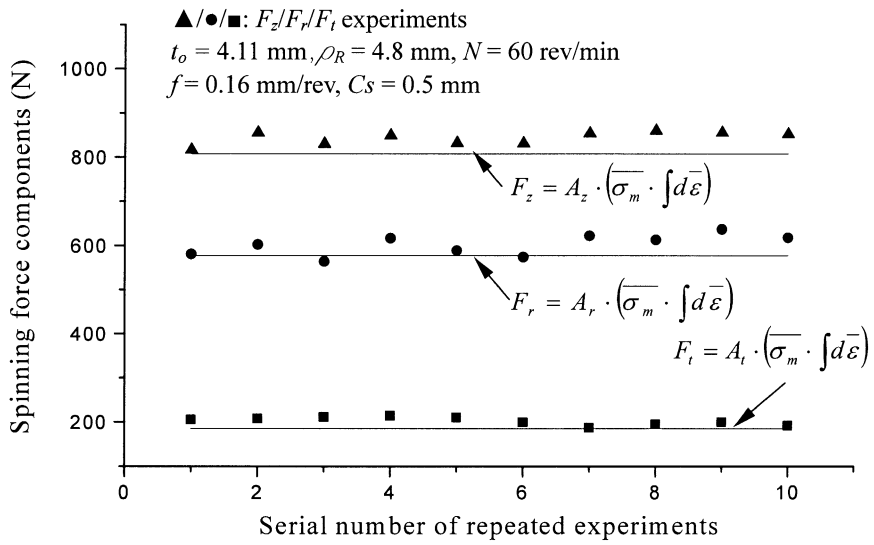

Fig. 13. Spinning force components vs. the serial number of repeated experiments.

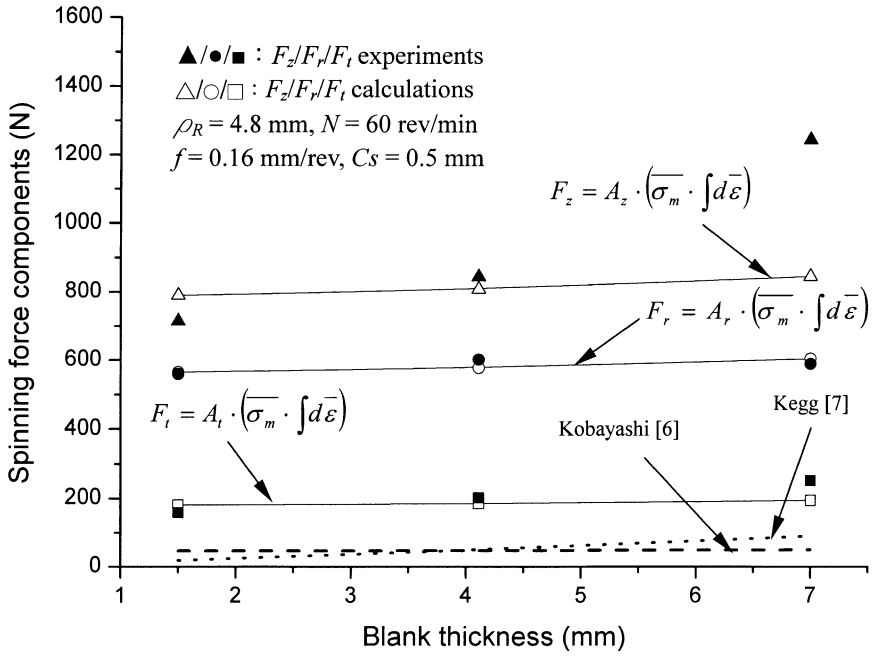

Fig. 14. Spinning force components as function of blank thickness.

for the experimental value F_z at $t_0 = 7.0\,\text{mm}$ is much larger than the calculation may be due to the spinning force is approaching the machine limit. In addition, Fig. 15 demonstrates the effect of over-roll factor on spinning force components. When $t_0 = 4.11\,\text{mm}$, $\rho_R = 4.8\,\text{mm}$,

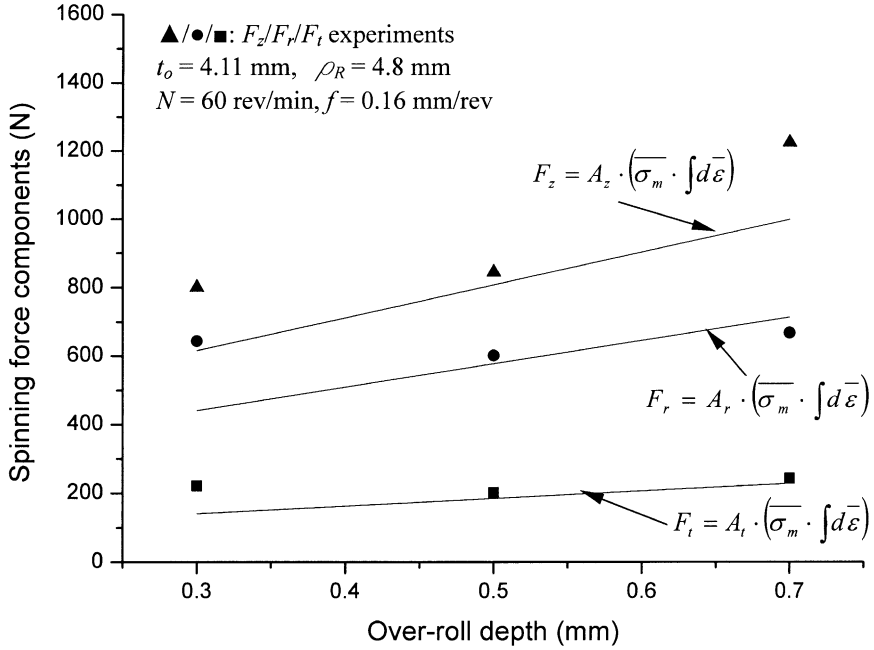

Fig. 15. Over-roll depth effect on spinning force components.

$N = 60\,\text{rev/min}$ and $f = 0.16\,\text{mm/rev}$, the greater over-roll depth means deeper contact between roller/blank, thus the force exerted by the roller of course increases. But from the experimental results, we noticed that the circumferential and radial force components for $Cs = 0.5\,\text{mm}$, were smaller than $Cs = 0.3\,\text{mm}$. This may be explained by the fact that, during the spinning process, a very thin oxide layer accumulated on the roller nose/blank contact area. When the roller presses on the blank, it causes this oxide layer to crack. If the over-roll is deep enough, the whole oxide layer tends to shear-off, which in turn reduces the shear force. When over-roll depth is set deeper than 0.5 mm, the reduction of force caused by the shear-off of the oxide layer is more than compensated by the greater amount of energy required by the deformation of the blank, thus the force increases again. Fig. 16 illustrates the circumferential force component with respect to roller nose radius. While $t_0 = 2.59\,\text{mm}$, $N = 40\,\text{rev/min}$, $Cs = 0.5\,\text{mm}$, $f = 0.13\,\text{mm/rev}$. (index of ■) and $f = 0.18\,\text{mm/rev}$. (index of •), it reveals that in the calculation, the dependence on the roller nose radius is much more apparent than in the experiment, however, both the prediction and the experimental results show that the circumferential force component increases with roller nose radius, since larger nose radius induces larger contact area and thus required larger force. Furthermore, the faster roller feed needs more energy to deform the material at unit revolution, thus increases the spinning force. Finally, Fig. 17 depicts the circumferential force components relative to the roller feed. At fixed $t_0 = 4.11\,\text{mm}$, $\rho_R = 4.8\,\text{mm}$, $N = 60\,\text{rev/min}$ and $Cs = 0.5\,\text{mm}$, the larger roller feed produces

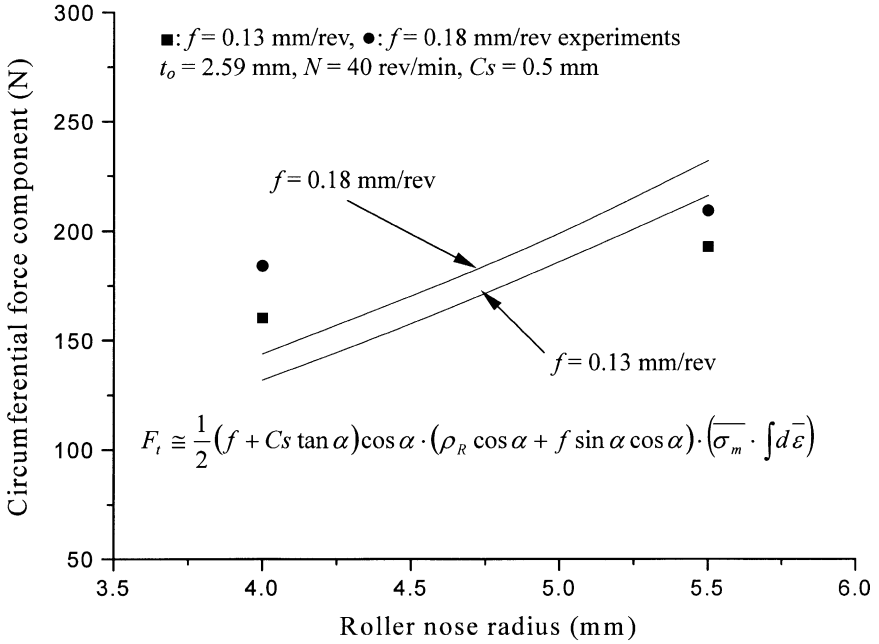

Fig. 16. Circumferential force component with respect to roller nose radius.

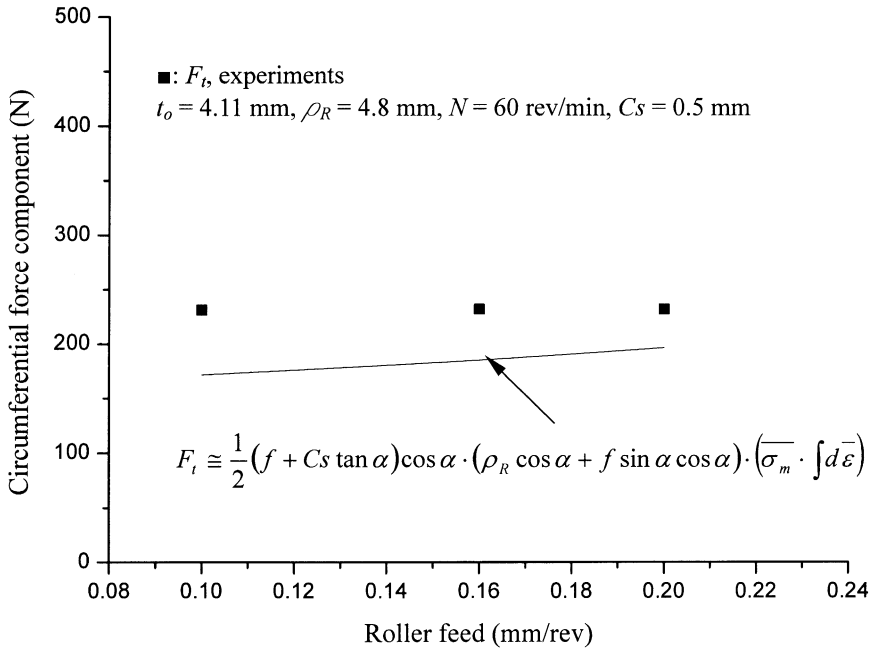

Fig. 17. Circumferential force component relative to the roller feed.

larger contact length which in turn induces larger contact area, thus higher spinning force. However, the increase in the circumferential force is not obviously, since the roller feed is small in the range of 0.1 and 0.2 mm/rev.

5. Conclusions

In this study of the analysis of shear spinning force, the following conclusions have been drawn.

1. An analytical model incorporating over-roll of the blank is proposed for the calculation of shear spinning forces.
2. The equations derived contain five parameters of the shear spinning process, namely blank thickness, roller nose radius, mandrel revolution, roller feed and over-roll depth. The effect of these parameters on shear spinning forces is discussed.
3. Shear spinning force calculated from equations derived in this study yield optimum results when over-roll of the blank is taken place in the process.

Appendix A. Referring to Fig. 4

$$\overline{AQ'_n}^2 = \overline{AQ_nAC},$$

$$(\overline{R_n\theta'_0})^2 = (2\rho_n - \gamma Z'_n)\gamma Z'_n = 2\rho_n\gamma Z'_n - (\gamma Z'_n)^2,$$

$$\rho_n \approx \frac{(\overline{R_n\theta_0}')^2}{2\gamma Z'_n} \approx \frac{(\overline{R_n\theta_0})^2}{2Z'_n},$$

$$\tan\delta' = \frac{\overline{AQ'_n}}{\overline{AO}} = \frac{\overline{R_n\theta'_0}}{\rho_n - 2\gamma Z'_n} = \frac{\overline{R_n\theta'_0}}{(\overline{R_n\theta'_0})^2 - 2\gamma^2 Z'^2_n/2\gamma Z'_n} \approx \frac{\overline{R_n\theta'_0}2\gamma Z'_n}{(\overline{R_n\theta'_0})^2} \approx \frac{2Z'_n}{R_n\theta_0}.$$

Appendix B. The derivation of Eq. (25)

Referring to Fig. 5, the following relationships are obtained:
Transformation: $0(x, y, z) \to 0'(x', y', z')$

$$x = x'\cos\psi - z'\sin\psi - \frac{D_R}{2},$$

$$y = y'$$

$$z = x'\sin\psi + z'\cos\psi. \tag{B.1}$$

A torus body equation:

$$\left[\sqrt{x^2+y^2}-\frac{D_R}{2}\right]^2-\rho_R^2+z^2=0 \tag{B.2}$$

or

$$\left[\sqrt{\left(x'\cos\psi-z'\sin\psi-\frac{D_R}{2}\right)^2+y'^2}-\frac{D_R}{2}\right]^2-\rho_R^2+(x'\sin\psi+z'\cos\psi)^2=0 \tag{B.3}$$

trace of roller sectioned by the plane PP. By substitution of $z'=z_0'$ into Eq. (B.3),

$$\left[\sqrt{\left(x'\cos\psi-z_0'\sin\psi-\frac{D_R}{2}\right)^2+y'^2}-\frac{D_R}{2}\right]^2-\rho_R^2+(x'\sin\psi+z_0'\cos\psi)^2=0. \tag{B.4}$$

Lengths a and b: substituting $y=0, z_0=r_1=\rho_R-f\cos\alpha$ and $x=0, z_0=r_1=\rho_R-f\cos\alpha$ into Eq. (B.4), we get

$$a=\sqrt{r_0^2-r_1^2}=\sqrt{\rho_R^2-(\rho_R-f\cos\alpha)^2}, \tag{B.5}$$

where $r_0=\rho_R$ and

$$\left[\sqrt{\left(0-r_1\sin\psi-\frac{D_R}{2}\right)^2+b^2}-\frac{D_R}{2}\right]^2-\rho_R^2+(0+r_1\cos\psi)^2=0,$$

$$b^2=\rho_R^2-r_1^2+D_R\left[\sqrt{\rho_R^2-(r_1\cos\psi)^2}-r_1\sin\psi\right],$$

where $r_1=\rho_R-f\cos\alpha$

$$b^2=D_R\left\{\sqrt{\rho_R^2-[(\rho_R-f\cos\alpha)\cos\psi]^2}-[(\rho_R-f\cos\alpha)\sin\psi]\right\}+\rho_R^2-(\rho_R-f\cos\alpha)^2$$

the roller trace equation

$$\left(\frac{x_0'}{a}\right)^2+\left(\frac{y_0'}{b}\right)^2=1 \tag{B.6}$$

the cross section of cone contact with roller

$$x_0'^2+y_0'^2=2R_0|x_0'| \tag{B.7}$$

solving the equations of (B.6) and (B.7)

$$(b^2-a^2)x_0'^2=a^2b^2-2a^2R_0|x_0'|,$$

substituting $K = a^2R_0/(b^2 - a^2)$, we get

$$(x_0' + K)^2 = \frac{a^2b^2}{b^2 - a^2} + K^2,$$

$$|x_0'| = \sqrt{\frac{a^2b^2}{b^2 - a^2} + K^2} - K,$$

$$|x_0'| = \frac{R_0}{(b^2/a^2) - 1}\left[\sqrt{\left(\frac{b}{R_0}\right)^2\left(\frac{b^2}{a^2} - 1\right) + 1} - 1\right], \tag{B.8}$$

$$\overline{\theta_0} = \cos^{-1}\left(\frac{R_0 - |x_0'|}{R_0}\right),$$

$$\overline{\theta_0} = \cos^{-1}\left[\frac{(b^2/a^2) - \sqrt{1 + (b/R_0)^2(b^2/a^2 - 1)}}{(b^2/a^2) - 1}\right]. \tag{B.9}$$

References

[1] Held M. Determination of the material quality of copper shaped charge liners. Propellants, Explosives, Pyrotechnics 1985;10:125–8.
[2] Hayama M, Kudo H, Shinokura T. Study of the pass schedule in conventional simple spinning. Bulletin of the JSME 1970;13(65).
[3] Hayama M. Rotary forming—from rolling and spinning. Tokyo, Japan: Japanese Plastic Process Association, Corona Co.; 1990.
[4] Avitzur B, Yang CT. Analysis of power spinning of cones. Journal of Engineering for Industry, Transactions of the ASME 1960;82:231–45.
[5] Kalpakcioglu S. On the mechanics of shear spinning. Journal of Engineering for Industry. Transactions of the ASME Series B 1961;83:125–30.
[6] Kobayashi S, Thomsen EG. A theory of shear spinning of cones. Journal of Engineering for Industry. Transactions of the ASME 1961;83:485–95.
[7] Kegg RL. A new test method for determination of spinnability of metals. Journal of Engineering for Industry. Transactions of the ASME 1961;83:119–24.
[8] Mielnik EM. Metalworking sciences and engineering. New York: McGraw-Hill, Inc.; 1993. p. 731–2.